





## Research Article

# Comprehensive Approach to Mitigating Solar Photovoltaic Power Penetration Effects in a Microgrid

Youngil Kim <sup>1</sup>, Manef Bourogaoui <sup>2,3</sup>, Azeddine Houari <sup>4</sup>, and Hyeok Kim <sup>5</sup>

<sup>1</sup>Department of Electrical and Computer Engineering, The George Washington University, Washington DC 20052, USA

<sup>2</sup>Université de Tunis El Manar, Ecole Nationale d'Ingénieurs de Tunis, Laboratoire des Systèmes Electriques, LR11ES15, 1002, Tunis, Tunisia

<sup>3</sup>Université de Carthage, Institut Supérieur des Technologies de l'Information et de la Communication, 1164, Ben Arous, Tunisia

<sup>4</sup>Nantes Université, Institut de Recherche en Énergie Électrique de Nantes Atlantique, IREENA, UR 4642, F-44600 Saint-Nazaire, France

<sup>5</sup>School of Electrical and Computer Engineering, University of Seoul, Seoul 02504, Republic of Korea

Correspondence should be addressed to Manef Bourogaoui; [manef.bourogaoui@enit.utm.tn](mailto:manef.bourogaoui@enit.utm.tn) and Hyeok Kim; [hyeok.kim@uos.ac.kr](mailto:hyeok.kim@uos.ac.kr)

Received 28 November 2021; Revised 8 June 2022; Accepted 22 July 2022; Published 10 October 2022

Academic Editor: Kamran Iqbal

Copyright © 2022 Youngil Kim et al. This is an open access article distributed under the Creative Commons Attribution License, which permits unrestricted use, distribution, and reproduction in any medium, provided the original work is properly cited.

High solar photovoltaic (PV) penetration in the electrical grid can result in undesired effects on the voltage quality, leading to line loss and voltage magnitude increases. One of the main criteria to ensure the safe penetration of high-power solar systems in the main grid is maintaining an acceptable voltage magnitude when a disturbance occurs (e.g., 0.95 and 1.05 per unit) with respect to total installed power generation capacity of PV power plants. This manuscript analyzes the effects of high solar PV penetration per unit of voltage stability using the Fast Voltage Stability Index and total power loss. Moreover, we investigate the flexibility benefits of coordinated voltage control based on a smart inverter of solar PV capacitor banks (SI-CBs) under five cases in a typical microgrid (MG) test model. For the test of the SI-CBs, MG modeling is developed on a modified IEEE 123 test feeder, which includes 11 building load solar PVs with smart inverters and capacitor banks with real-time data from an area in Los Angeles, California, USA. The simulation results are presented to validate the effectiveness of the proposed approach using a real-time MATLAB interface to the Open Distribution System Simulator (OpenDSS).

## 1. Introduction

Microgrids (MGs) are emerging as critical tools for resilience with distributed energy resources, which have been increasing in the US grid. As one of the world's largest and most complex human-made systems, MGs are highly vulnerable to three types of external threats: (1) natural disasters, (2) physical attacks, and (3) cyberattacks [1–3]. Therefore, extensive studies have been conducted on MGs to ensure their stability and reliability in supplying electrical power with many intermittent renewable energy resources [4–10]. In Ref. [4], the Bronzeville neighborhood of Chicago is considered to present a way to achieve MG integration into the existing distribution management system based on advanced design, control, and test approaches. In Ref. [5], a highly fluctuating load case is considered for modeling an

MG power generation cost function, where a real-time monitoring operation is proposed considering practical cases of wind speed, solar irradiance, and battery charge states. Thus, resonance frequency monitoring was the subject of Ref. [7], in which a novel algorithm was proposed based on the wavelet transform, and several cases were considered, such as MG islanded and connected modes.

According to IEEE Standards 1547 and 929 [11, 12], some measures should be considered to ensure the reliability and stability of the grid-tied MG operations and allow integrating more distributed generation (DG)-based renewable energy resource MGs. As a source of renewable energy resources in MGs, solar photovoltaics (PVs) can steadily provide power when the grid is down and reduce energy costs when the grid is available in the US [13]. In addition, the sizing of MG components, such as the PV, battery, and

generator capacities, is a paramount issue, as presented in Ref. [14]. The main advantages of solar PV grid integration include the potential of improved power quality and grid reliability and reduced transmission and distribution loss [15, 16], as there is a growing demand for alternative clean energy vs. fossil fuel. However, the integration of solar PV in weak distribution networks can often cause overvoltage problems during higher-level penetration scenarios. Traditionally, overvoltage problems have been mitigated using passive methods, such as network reinforcement, leading to high DG interconnection costs [17]. Furthermore, higher-level solar PV penetration scenarios have been becoming increasingly common in studies because of the potential to affect the life cycle of the operation of the distribution feeder equipment and the increased maintenance costs [18].

Therefore, voltage problems, such as overvoltage or voltage drop, in the distribution network with the penetration of PVs and MGs have been addressed in the literature through impact analyses to develop novel schemes of coordinating voltage control leading to increased PV generation [18, 19]. Table 1 presents a comprehensive review of such impact analyses [20–22] or coordinate strategies [23–28] of Open Distribution System Simulator (OpenDSS) modeling during solar PV penetration. For example, in Ref. [20], patterns from real measurements were used for a probabilistic load model, and the irradiance, temperature, and load values at each time step were processed in MATLAB and sent to OpenDSS to calculate the three-phase power flow. The model was tested with the comprehensive test feeder, and an error of 2.78% was obtained compared with the original results. Thus, the voltage variation issue due to the solar generation intermittency was the subject of [26], where OpenDSS and MATLAB were used to simulate the proposed feeder over 24 hours. Accordingly, a PI-based voltage control method is suggested to reduce the voltage deviations at the PCC of the PV inverters. In summary, OpenDSS modeling from MATLAB [20, 21, 23, 24, 26–29] or CYMDIST [25] through COM server was used in the modified IEEE test feeder 7 [28], 13 [21, 23, 25, 27], 17 [29], 34 [26], 55 [24], and 69 [29] and in American Electric Power (AEP) 12.4 kV [22].

Moreover, to make various cases and a detailed impact analysis during high PV penetration, a chronological Monte Carlo [20] and quasistatic time series [21] were used to analyze the voltage profile that interferes with standard voltage regulation practices [30] and loss [22, 24–26], maintaining the voltage limit (voltage profile) [20–22, 24–26, 28], maximization user profits, and cost minimization [23, 27, 29]. Some approaches maintain the network voltage at an acceptable level using PI control based on Q/P control [26], autonomous coordinate voltage control [24], and conservation voltage reduction algorithms [27] to realize these voltage regulation issues. Some methods maximize the customer benefit based on operation constraints using model predictive control [23] or dynamic programming [25] in OpenDSS modeling. Works in Ref. [31] consider an IEEE 13 nodes test feeder including solar PV generation and distribution static compensator so as to perform harmonic mitigation and

power quality analysis. In order to validate the control of the distribution static compensator, several scenarios are considered to investigate disturbances of power quality and harmonics, like insolation of solar radiation, outage of PV plant from grid, and synchronization of PV plant to grid. The purpose of [32] is the amelioration of risks related to solar photovoltaic (PV) systems integration into a commercial electric power grid and the presentation of their mitigation strategies; thereby, two common risk modeling approaches are compared [33]. It is a review about the theoretical works and industrial applications of hybrid AC/DC distribution systems through analyzing their efficiency and energy loss; then, the study can be considered for future research regarding the mitigation of PV energy penetration. In addition, more methods, used to overcome instability issues caused by high penetration of photovoltaic (PV) systems in low-voltage distribution networks (LVDNs), are presented in Ref. [34]. The contributions and shortcomings of the different methods are compared, when dealing with high penetration of PV units in the LVDNs to handle the impact of the overvoltage. These methods are as follows: energy storage systems (ESSs) by storing excess energy through batteries during the integration of high penetration of PVs and low load levels, load side management (LSM) by adjusting or controlling power consumption from peak to peak, reactive power support (RPS) by controlling the amount of reactive power by PV inverters through droop control strategy, active power curtailment (APC) in PV inverters to deal with a negative impact of voltage fluctuation that resulted from power intermittency, and grid reinforcement (GR) by changing the network structure to reduce the voltage rise challenge.

The main contributions of the paper, with respect to the existing works described above, are as follows:

- (i) The paper investigates the issue of high PV penetration effects with respect to the total installed power generation capacity of PV power plants in the MG and presents a coordinating voltage control solution to maintain the voltage limits of  $V_{\min}=0.95$  and  $V_{\max}=1.05$ , which were chosen according to the ANSI standard.
- (ii) The current existing work with OpenDSS COM interface with MATLAB has only been small size of IEEE model less than 73 such as IEEE 7 [28], 13 [21, 23, 27], 17 [29], 55 [24], and 73 [20] because of the required complex interface skills. However, we have proposed the bigger MG model-based IEEE 123 model compared to the existing work.
- (iii) In the existing similar works of our topic with OpenDSS-MATLAB [21, 23, 24, 27–29], there are three papers, which deal with voltage stability in terms of PU [20, 21, 28]. In addition, there are no cases as extreme cases. However, our paper has more extremely cases such as 45, 60%, 100%, and 200% compared to 10% [20] as well as tried to analyze on the impact of distributed PV in terms of

various indicators as power losses, FVSI, and voltage stability compared with other 3 cases.

- (iv) A new coordinated voltage control, combining two control techniques using smart inverters and capacitor banks, is implemented with the integration of different indexes like mentioned above, leading to a new control algorithm approach different from the existing methods in the open literature as described in [22, 27, 31, 34].
- (v) The studied MG architecture considers real data from Los Angeles, California, such as the weather conditions and commercial building data. The MG is a modified version of the IEEE test feeder 123 and was simulated using OpenDSS. The results were exported to MATLAB using the COM interface [19].
- (vi) Different scenarios are considered for testing the robustness of the proposed coordinated voltage control.
- (vii) A comprehensive approach is proposed, highlighting the steps to achieve a hybrid simulation between OpenDSS and MATLAB and validate the proposed coordinate voltage control.

The rest of the paper is organized as follows. Section 2 presents the configuration of grid-tied MG operations, which include solar PV with different building loads for OpenDSS modeling. Section 3 describes the system framework of the OpenDSS tool COM interface with MATLAB. Section 4 provides the proposed coordinated voltage regulation control strategy of the PV smart inverter (SI) with capacitor banks (CBs). Finally, Section 5 evaluates the simulation results for the proposed system in various cases.

## 2. Microgrid Configuration

In this paper, the IEEE 123-node test feeder is employed to study the issue of voltage violation due to the high level of solar PV energy penetration. The detailed parameters of the IEEE 123 test model are described in Table 2. The technical details are given in a separated document and can be found at IEEE PES test feeder website [19]. The feeder is a composition of three MGs, separated by different switchers,  $SW_1, \dots, SW_5$ , as indicated in Figure 1. Several commercial buildings and solar PV power plants were added to the feeder at different locations. The objective is to study the feeder operation using real-time data for the load in different building types and solar irradiance. The data on the electric power consumption of the buildings were provided by the Department of Energy [30]. Thus, solar irradiance can be extracted using the PVGIS website [35].

In total, 10 PV power plants were added to the IEEE 123-node feeder, with a total of power generation capacity of 10 MVA, presented in Figure 1. In this case, the PV power plants supply and support the whole feeder, including the commercial buildings. The main objective is to study and analyze the effect of the PV energy penetration in the proposed MGs.

All data from the Los Angeles area are considered part of the case study for this paper (Figure 2).

The temperature inside the cell module is estimated based on the thermal model provided by [36]

$$T_c = T_m + \frac{Ir}{I r_0} \cdot \Delta T. \quad (1)$$

The value of the back-surface module temperature  $T_m$  can be calculated using (2). The environmental conditions, namely, solar irradiance, wind speed, and ambient temperature measurements, are employed to calculate the back-surface temperature. These measurements are found in recognized databases, such as NASA and PVGIS [35, 37]:

$$T_m = Ir \cdot (e^{a+b \cdot WS}) + T_a. \quad (2)$$

Two coefficients,  $a$  and  $b$ , should be determined empirically, and the temperature difference between the cell and module back-surface must be calculated to determine the back-surface temperature. The values were chosen for polymer, thin-film, or steel PV technologies, according to Ref. [25]. Therefore, the PV power output is calculated using

$$P_{PV} = P_{mpp} \cdot Ir \cdot f. \quad (3)$$

Figure 3 displays the PV power generation under the influence of the weather conditions: temperature, wind speed, and irradiance.

We analyzed the annual load consumption for each type of building used in the MG model. Table 3 lists different types of loads ordered from highest to lowest for the annual load consumption for each building, which is from the load consumption of the interior equipment, fans, cooling, and interior lights. In most cases, the interior equipment and lights contribute to the largest load consumption.

Furthermore, Figure 4 illustrates the combined annual power-sharing between different load types for all buildings. Despite being the primary consumption source for only the HOS, a significant amount of energy is consumed by cooling appliances.

The different building load behaviors are assessed and validated through the OpenDSS, an electric power distribution system simulator supporting distributed energy resource grid integration and grid modernization. Figure 5 presents the hourly consumption profiles for real and reactive power for each building for two days in January 2015.

## 3. Implementation of OpenDSS COM Interface with MATLAB

In this paper, the simulation framework chosen for the MG model is OpenDSS, developed by the Electric Power Research Institute [38]. It is widely used in the industry to simulate large- and small-scale balanced/unbalanced networks, yielding comprehensive support documentation [39]. It is up-to-date software following the electric grid modeling and analysis needs, specifically those related to the vast amount of renewable energy generation and penetration, smart grid applications in the modern utility grids, and harmonic analyses.

This software was chosen for several reasons. First, it is free and open source, making the model easily transferable, modifiable, and updatable as needed. Furthermore, its COM server

TABLE 1: Case study summary for Open Distribution System Simulator (OpenDSS) microgrid (MG) modeling during high photovoltaic (PV) penetration.

Reference	Model	Tool	Objective	Approach	Duration
Marulanda and Pavas [20]	IEEE 73 test bus feeder (comprehensive test feeder—Kersting)	OpenDSS with MATLAB	Analyze the power flows and voltage profile of the feeder with 10.16% PV generation	Chronological Monte Carlo simulation for distribution systems with PV generation	24 hours
Ahamioje and Krishnaswami [21]	IEEE 13 bus feeder	OpenDSS, MATLAB, and Grid PV with GIS	Design on the model the likely real effects of PV on operations	Quasi-static time series analysis with dynamic volt/var and active power control with Grid PV toolbox integration of geographical information	180 hours
Solanki et al. [22]	12.47 kV distribution feeders for American electric power (AEP)	OpenDSS	Investigate the effects of high PV penetration with cloud cover scenarios as percentage system loss and voltage variation	Changing the regulator/LTC tap settings, reconductoring distribution lines, changing the placement of capacitor banks, employing storage to efficiently manage the dispatch of PV system	24 hours
Ma et al. [23]	IEEE 13 test bus feeder	OpenDSS with MATLAB (optimization tool)	Optimizing the generation cost to minimize operation cost	Model predictive control	24 hours
Pukhrem [24]	IEEE 55 test bus feeder (European LVDN)	OpenDSS with MATLAB	Alleviate the voltage fluctuation and reduce the overall P/Q network loss against the extreme-case scenarios	Autonomous coordinated voltage control techniques of grid-tied PV inverters	24 hours (every 5 min)
Ramachandran [25]	IEEE 13 node test feeder with PV at the end node	OpenDSS and CYMDIST	Determine optimal bids to maximize its profit and the effects of voltage imbalance and loss of the feeder	Dynamic programming	24 hours
Nowak et al. [26]	IEEE 34 test feeder	OpenDSS and Grid PV toolbox in MATLAB for PV inverters	Simulated on PV bus V, P, and Q based on a) maximum standard deviation via distance from the substation, b) total energy loss (kWh) in the feeder via penetration, and c) size difference of PV inverter for voltage PV based on normalized V	PI-based reactive power control method of PV inverters	24 hours
Liu and Overbye [27]	IEEE 13 node test feeder	OpenDSS and MATLAB	Find an operating point that maximizes energy savings after minimizing the total system loss and system energy consumption	Conservation voltage reduction algorithm from SQP to minimize the deviation from the control voltage level	4 hours
Liu et al. [28]	IEEE 7 node test feeder	MATLAB and OpenDSS	Increase PV hosting capacity with different voltage problems	Voltage/var control and voltage/watt control for a smart inverter	
Ammar and Sharaf [29]	IEEE test feeder 17 buses (25 kV) and IEEE test feeder 69 buses (12.66 kV)	MATLAB and OpenDSS	Minimize the deviation of the distribution network voltages	Finding optimal coordinated PV generator reactive power and HV/MV OLTC settings throughout the optimization time frame	

TABLE 2: MG parameter configuration.

Microgrids	Number	3
Nodes	Number	123
Switches	Number	11
Lines	Number	117
	Length range (min-max) (ft.)	100–1000

TABLE 2: Continued.

Transformers	Number	13	
	KVA power	Substation—Bus 150–115-D/4.16 Gr-W (KV)	5000 (KVA)
		XFM-1—Bus 610–4.16-D/0.48-D (KV)	150 (KVA)
		T11—Bus 11–2.4-W/0.24-W (KV)	100 (KVA)
		T46—Bus 46–2.4-W/0.24-W (KV)	1000 (KVA)
		T114—Bus 114–2.4-W/0.24-W (KV)	200 (KVA)
		T6—Bus 6–2.4-W/0.24-W (KV)	150 (KVA)
		T22—Bus 22–2.4-W/0.24-W (KV)	1500 (KVA)
		T59—Bus 59–2.4-W/0.24-W (KV)	1500 (KVA)
		T50—Bus 50–2.4-W/0.24-W (KV)	1500 (KVA)
		T39—Bus 39–2.4-W/0.24-W (KV)	1500 (KVA)
T88—Bus 88–2.4-W/0.24-W (KV)	1500 (KVA)		
T71—Bus 71–2.4-W/0.24-W (KV)	1500 (KVA)		
T75—Bus 75–2.4-W/0.24-W (KV)	1500 (KVA)		
Shunt capacitors	Number	4	
	KVAR power	C83—Bus 83	600 (KVAR)
		C88—Bus 88	50 (KVAR)
		C90—Bus 90	50 (KVAR)
C92—Bus 92		50 (KVAR)	
Regulators	Number	4	
	KVA power	Reg1—Bus 150–2.4-W/2.4-W (KV)	5000 (KVA)
		Reg2—Bus 9–2.4-W/2.4-W (KV)	2000 (KVA)
		Reg3—Bus 25–2.4-W/2.4-W (KV)	2000 (KVA)
Reg4—Bus 160–2.4-W/2.4-W (KV)		2000 (KVA)	
Commercial loads	Number	11	
PV power plants	Number	6	
	Total capacity (MVA)	PV1 to PV10 (bus connection in Figure 1)—2.4 kV	10 (MVA)
Smart inverters	Number	6	10

has extensive cosimulation capabilities, allowing a driver program to run the simulation from almost any programming language/environment. In this paper, the driver is used in MATLAB, and the OpenDSS executive is described in Figure 6.

In this work, the OpenDSS tool is hosted under MATLAB as the COM interface. Thus, several commands should be used to ensure communication between OpenDSS

and MATLAB. Most of these commands are described in Table 4. All commands can be found in Visual Basic for Applications-Distribution System Simulator (VBA-DSS) interface properties and methods under Excel software.

The following program structure can be followed when implementing the COM interface between OpenDSS and MATLAB.

```

% Starting the In-Process COM Server
DSSObj = actxserver ('OpenDSSEngine.DSS');
Start = DSSObj.Start (0);

% Define different interfaces
DSSText = DSSObj.Text;
DSSCircuit = DSSObj.ActiveCircuit;
DSSBus = DSSCircuit.ActiveBus;
DSSElement = DSSCircuit.ActiveCktElement;
DSSGenerators = DSSCircuit.Generators;
% Call and compile the DSS file
DSSText.command = 'compile "Folder_path\name_DSS_file.dss"';
% Define variables here
% Implement control algorithms
for time = ..... % all MATLAB programming language like
    % "while", "if", "switch case"...can be used
DSSCircuit.Solution.Solve;
% Add control algorithms here
End % Export and plot results

```

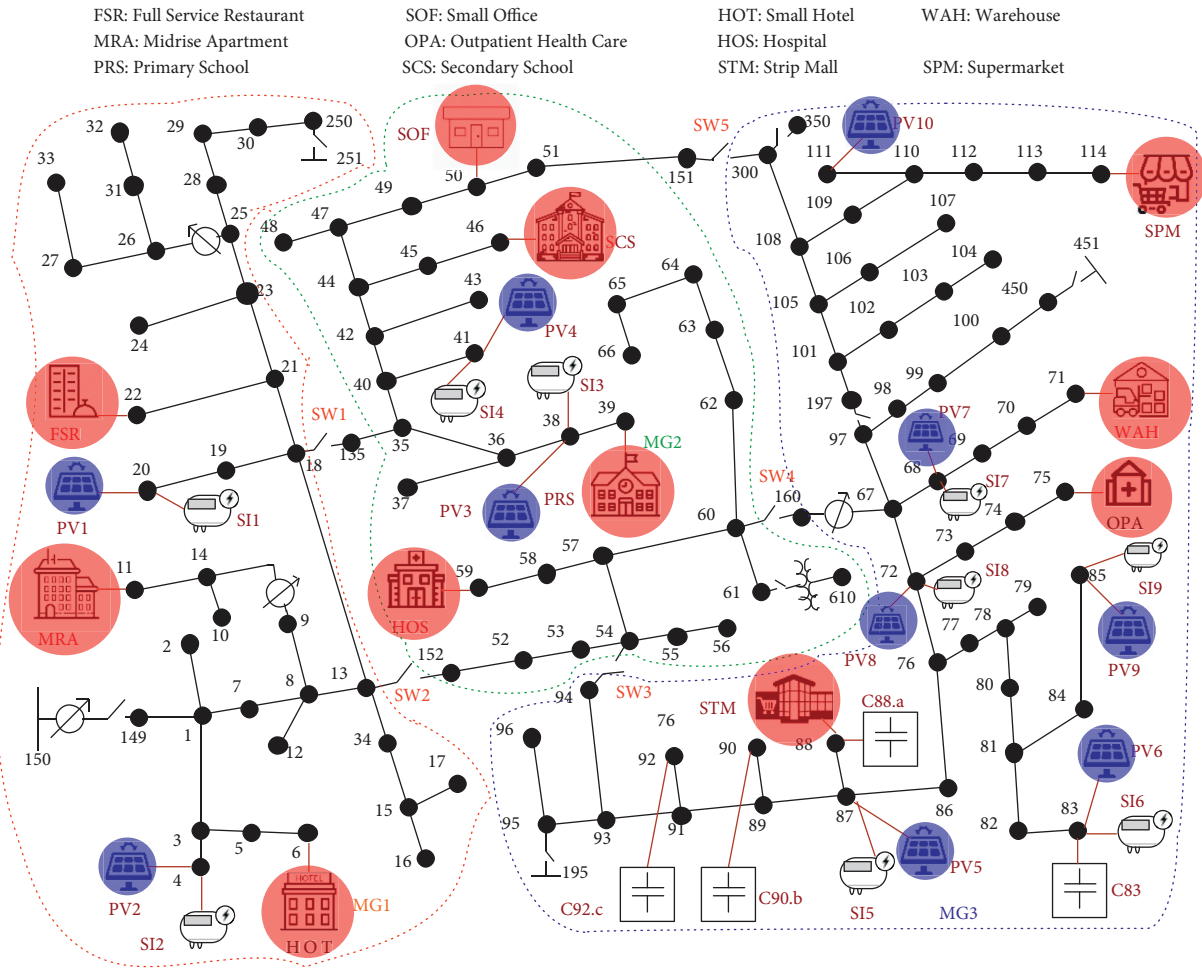


FIGURE 1: Microgrid configuration based on the IEEE 123-node test feeder.

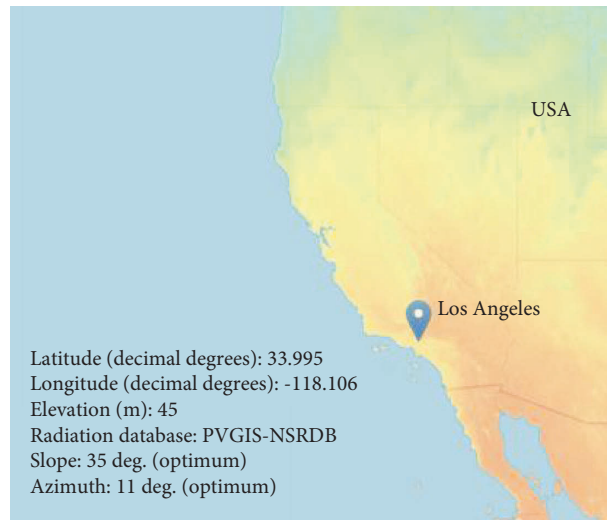


FIGURE 2: Selected location in Los Angeles using PVGIS [35].

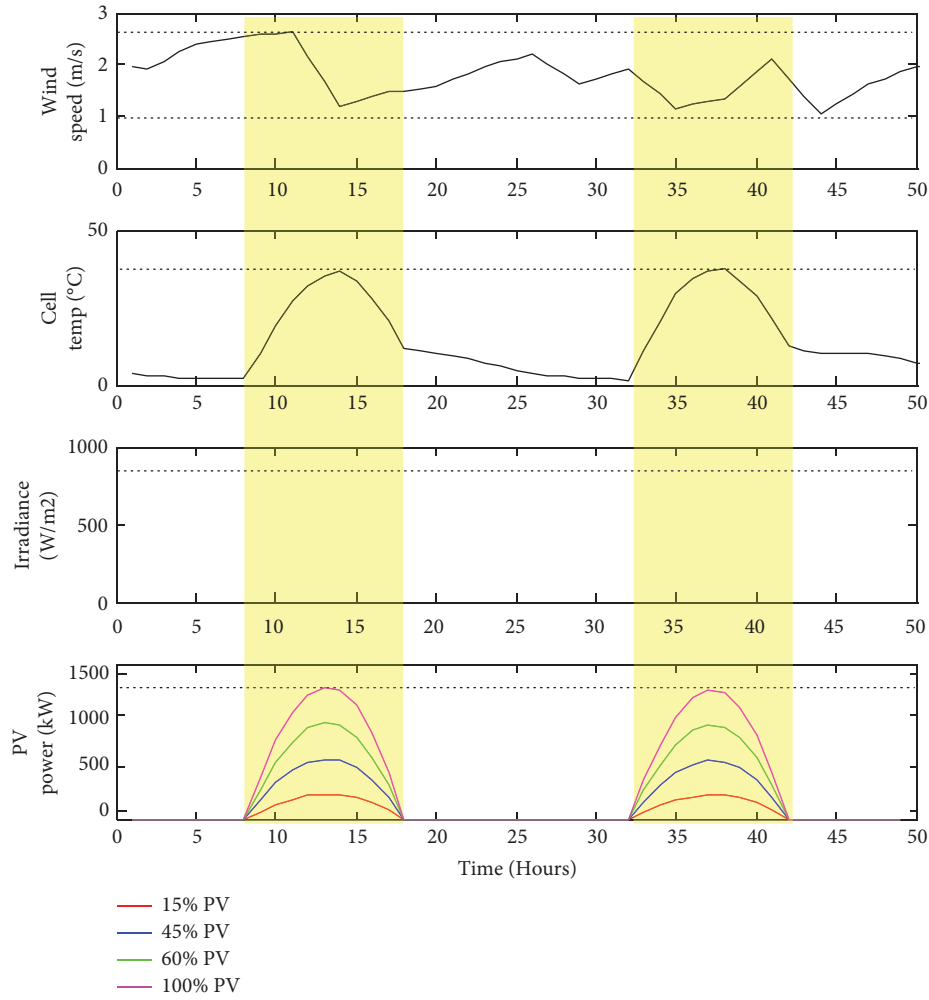


FIGURE 3: Influence of the weather conditions on the PV power generation.

TABLE 3: Annual MW consumption order of different loads by building.

Building	Order: 1	2	3	4
FSR	Interior equipment	Interior lights	Fans	Cooling
HOS	Cooling	Interior equipment	Interior lights	Fans
MRA	Interior equipment	Interior lights	Cooling	Fans
OPA	Interior equipment	Cooling	Fans	Interior lights
PRS	Interior lights	Interior equipment	Cooling	Fans
SCS	Cooling	Interior lights	Interior equipment	Fans
HOT	Interior equipment	Interior lights	Cooling	Fans
SOF	Interior equipment	Interior lights	Fans	Cooling
STM	Interior lights	Interior equipment	Fans	Cooling
SPM	Interior lights	Interior equipment	Fans	Cooling
WAH	Interior equipment	Interior lights	Fans	Cooling

#### 4. Mathematical Modeling (Problem Formulation)

This study considers a radial distribution feeder with  $n$  nodes, including the representative load and solar PV with SI for the IEEE 123 test feeder model. We used to Classical DistFlow Equations, which is to express the simplified equation in terms

of Power Flow. A well-recognized power solver called DistFlow is used to solve the power flow problems [40].

*4.1. Power Flow Analysis.* In Figure 7, node 1 represents the feeding substation whose voltage is assumed to be constant, whereas three different load-type models ( $P_{L,n}$ ,  $Q_{L,n}$ ) with

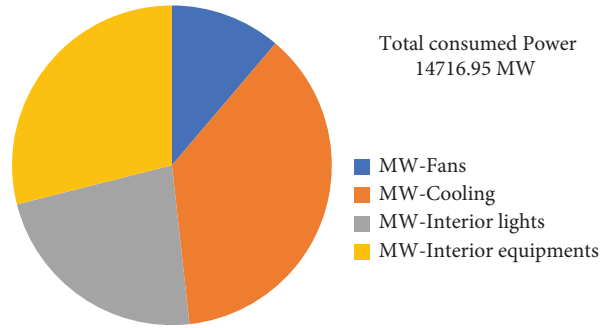


FIGURE 4: Annual consumption for each type of load.

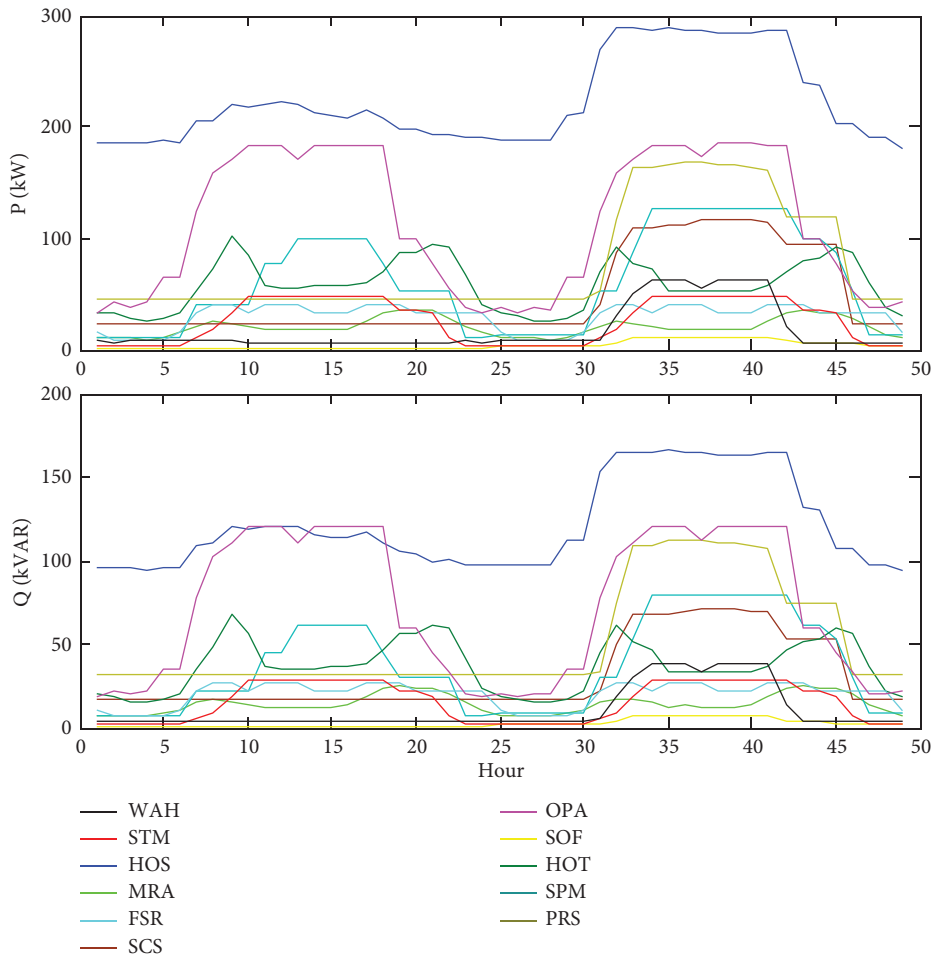


FIGURE 5: Hourly consumption by building for two days in January: (a) real power and (b) reactive power.

combination of Smart Inverter (SI) and Capacitor Bank (CB) are described as follows:

(1) Only PV ( $P_{PV,n}$ ,  $Q_{PV,n}$ ): active and reactive power from solar PV

(2) PV-SI ( $P_{PS,n}$ ,  $Q_{PS,n}$ ): active and reactive power from Smart Inverter of solar PV

(3) PV-SI-CB ( $P_{CB,n}$ ,  $Q_{CB,n}$ ): active and reactive power from the SI of solar PV with CB



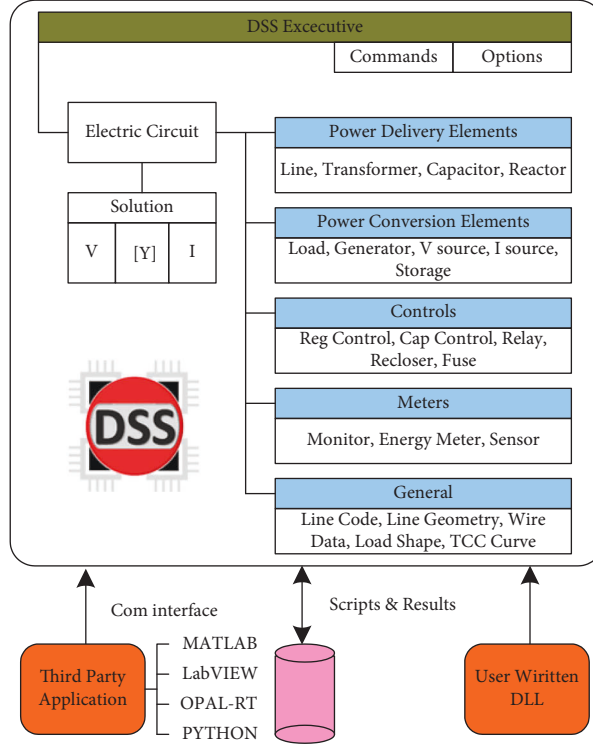


FIGURE 6: DSS executive of the OpenDSS [30].

The power flow equations with solar PV are given as follows [40]:

$$P_n = P_{n-1} - R_{n-1} \cdot \frac{P_{n-1}^2 + Q_{n-1}^2}{V_{n-1}^2} - P_{L,n-1} + P_{PV,n-1} + P_{PS,n-1} + P_{CB,n-1}, \quad (4)$$

$$Q_n = Q_{n-1} - X_{n-1} \cdot \frac{P_{n-1}^2 + Q_{n-1}^2}{V_{n-1}^2} - Q_{L,n-1} + Q_{PV,n-1} + Q_{PS,n-1} + Q_{CB,n-1}, \quad (5)$$

$$V_n^2 = V_{n-1}^2 - 2 \cdot (R_{n-1} \cdot P_{n-1} + X_{n-1} \cdot Q_{n-1}) - (R_{n-1}^2 + X_{n-1}^2) \frac{P_{n-1}^2 + Q_{n-1}^2}{V_{n-1}^2}. \quad (6)$$

The feeder section between nodes  $n$  and  $n-1$  could be expressed as  $R_n + jX_n$ . A higher power loss always occurs in the MG when increasing the number of PV installations incorporated into each circuit model. From the model, power loss in section  $n$  could be expressed as follows:

$$P_{\text{loss},n} = R_n \cdot \frac{P_n^2 + Q_n^2}{V_n^2}. \quad (7)$$

**4.2. Smart Inverter (SI) of Solar PV.** One of the significant effects of the DG is the reverse power flow, while the distribution grid should be designed to move electricity in one direction from large remote generators on the transmission system to customers. Reverse power flow generally occurs

when the generation of a distributed electric power plant exceeds the local load demand when  $\sum P_{PV,n} > \sum P_{L,n}$ , causing power to flow in the opposite direction than normal, which could make this feeder more vulnerable to voltage instability. The inverter can mitigate the reverse power flow by compensating for the reactive power [41]. The inverter must satisfy the relation  $\sqrt{P^2 - Q^2} \leq S$ , where,  $P$ ,  $Q$ , and  $S$  are inverter's real power output, var output, and rated capacity, respectively. Thus, the maximum var magnitude that can be injected or absorbed by the inverter of solar PV at any given time can be estimated as  $Q_{\text{max},n} = \sqrt{(S_n)^2 - (P_n)^2}$ . We used  $Q$ , which is related to the difference of apparent power and actual real power of the PV inverter as follows:

$$Q_{PV,n} = \sqrt{(S_{PV,n})^2 - (P_{PV,n})^2}. \quad (8)$$

**4.3. Capacitor Bank.** Let  $\varphi_n$  be the reactive power supplied by  $CB_n$  where  $n = 1, 2, 3, \dots, N$ , and  $N$  is the number of CBs.  $a_Q$  and  $a_V$  denote the weights associated with improving the power factor at the bus and reducing the voltage variation to maintain ANSI (0.95/1.05), respectively. The CBs could be calculated as follows [42]:

$$\sum_k^T \sum_n^N a_Q \cdot \varphi_n + a_V \cdot v_n. \quad (9)$$

**4.4. Index of Voltage Stability Using ANSI and Fast Voltage Stability Index.** For a couple of decades, voltage stability assessment has received increasing attention due to the

TABLE 4: DSS commands used under MATLAB [38].

Command	Description
DSSObj	Define the server
DSSObj. Text	“Text” interface ensures easy access to the text interface command and result properties. For example, the DSS Text. command = “OpenDSS command” allows implementing any command of OpenDSS under MATLAB
DSS Circuit. Solution	“Solution” interface allows the use of the common command “DSS solution. Solve” to solve the circuit
DSS Obj. Active circuit	“Active circuit” interface is vital for obtaining various quantities via the COM interface
DSS Circuit. Active CktElement	“Active CktElement” interface allows access to the properties of any circuit element set in the program
DSS Circuit. Active Bus	“Active Bus” interface provides the properties of the active bus
DSS Circuit. Generators	“Generators” interface allows access to the generator collection in the active circuit
DSS Circuit. Lines	“Lines” interface allows access to the line collection in the active circuit
DSS Circuit. Loads	“Loads” interface allows access to the load collection in the active circuit

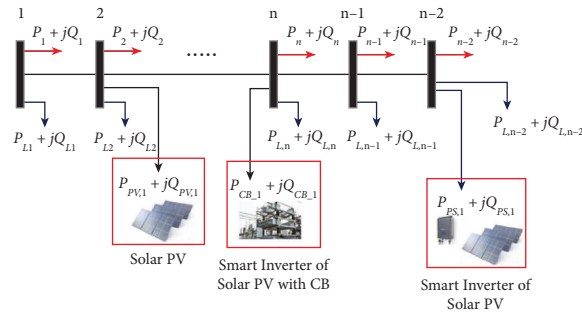


FIGURE 7: Modeling of a microgrid for power flow analysis.

complexity of power systems and integration of solar PV in the distribution system. In this work, the voltage stability index in each bus is evaluated using ANSI and the Fast Voltage Stability Index (FVSI). The network’s “PV hosting capacity” is defined as the maximum PV system size that does not exceed the network operating standards when interconnected to any valid bus. Thus, the voltage of all network buses must remain within the ANSI limits of  $0.95 \leq V_{pu} \leq 1.05$  in the steady state. We can estimate the maximum load for weak bus identification using the FVSI [43, 44]. Taking the symbols  $i$  as the sending bus and  $j$  as the receiving bus, FVSI can be defined as follows [43, 44]:

$$FVSI_{ij} = \frac{4 \cdot Z^2 \cdot Q_j}{V_i^2 \cdot X}, \quad (10)$$

where  $Z$  is the line impedance,  $X$  represents the line reactance,  $Q_j$  denotes the reactive power at the receiving end, and  $V_i$  indicates the sending end voltage. The general two-bus representation is illustrated in Figure 8.

The value of  $FVSI_{ij}$  should always be less than 1 to maintain the voltage stability in an MG, and if its value is greater than 1, the MG experiences a voltage drop, which can be controlled by regulating either the distributed energy resources or reactive power compensator [45].

## 5. Proposed Approach

The steps described by the flowchart are followed to maintain the voltage stability of the proposed MG

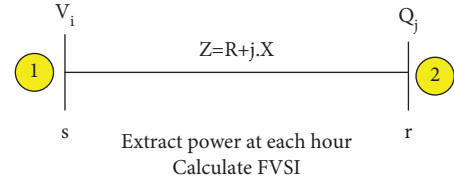


FIGURE 8: General two-bus representation for the fast voltage stability index.

configuration. After performing the power flow analysis, voltages at all nodes were extracted, and their values were compared to those defined by the ANSI limits (0.95 and 1.05 per unit). The SI control was performed to adjust the voltages if the voltage was not within these limits. Then, the voltage values were verified again if they did not respect the ANSI requirements, and the CBs were used to adjust their values. Finally, the FVSI and power loss were assessed to evaluate the performance of the proposed controls as shown in the Figure 9).

The algorithm of the SI is executed according to the following steps.

The CB control (part *b* of the flowchart) is based on the power factor adjustment. This power factor should be greater than 0.9 to compensate for the reactive power from the inductive load, maintaining the voltage within ANSI limits. However, the flowchart in Figure 10 (part a) details the SI control.

Step 1: Control the SI and extract the values of the active and reactive power of the PV power plant until  $j$

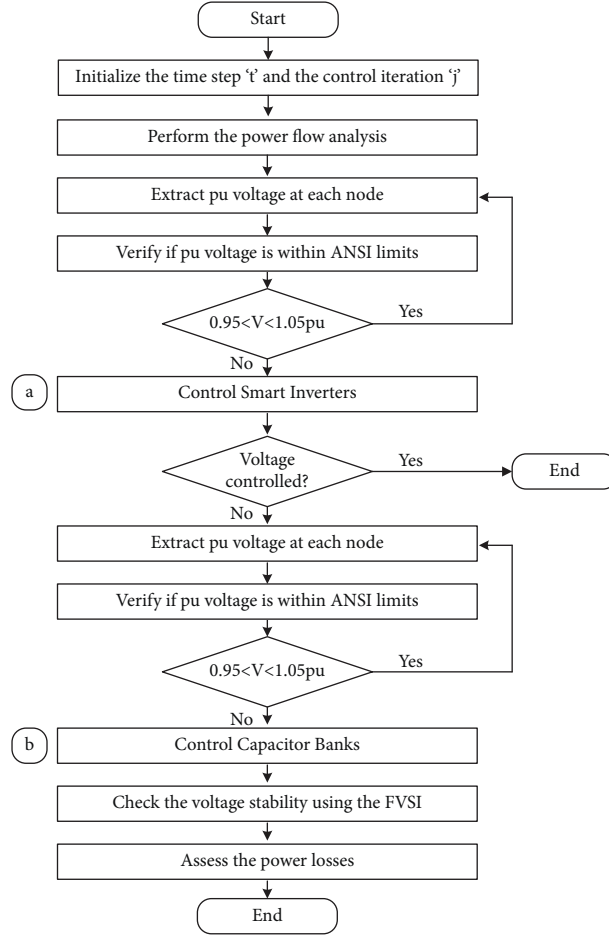


FIGURE 9: The proposed strategy for the microgrid control.

exceeds a defined control iteration  $j_{\max}$  through the following substeps:

- (a) Calculate the PV plant output power ( $P_{PV}$ ) based on the actual weather conditions using

$$P_{PV} = P_{\text{mpp}} \cdot I_r \cdot f. \quad (11)$$

{if  $P_{ac}(t-1) = 0$  (i.e., Status( $t-1$ ) = OFF and  $P_{dc}(t)$

$$\geq \frac{\%S_{r1} \cdot S_r}{100} = P_{dc1}(t), \quad \text{Status}(t) = \text{ON} \Big) \text{ else if } P_{ac}(t-1) > 0 \text{ (i.e., Status}(t-1) = \text{ON and } P_{dc}(t) \quad (12)$$

$$< \frac{\%S_{r2} \cdot S_r}{100} = P_{dc2}(t), \quad \text{Status}(t) = \text{OFF} \Big),$$

- (c) Calculate the inverter's desired active output power. When the inverter status indicates on, the active output power of the SI ( $P_{d,ac}(t)$ ) is calculated in

$$P_{d,ac}(t) = P_{dc}(t) \cdot E_{\text{Curve}}, \quad (13)$$

- (b) Check the inverter status: on or off.

The objective is to identify the inverter status of the previous iteration ( $t-1$ ) and change the status in the actual iteration ( $t$ ) based on

- (d) Check the inverter reactive power limits for the cases of provided and absorbed reactive power. The inverter reactive power limits  $Q_{L,ac}(t)$  depend on whether the desired reactive power  $Q_{d,ac}(t)$  is provided or absorbed (i.e., positive or negative) as illustrated by the following equation:

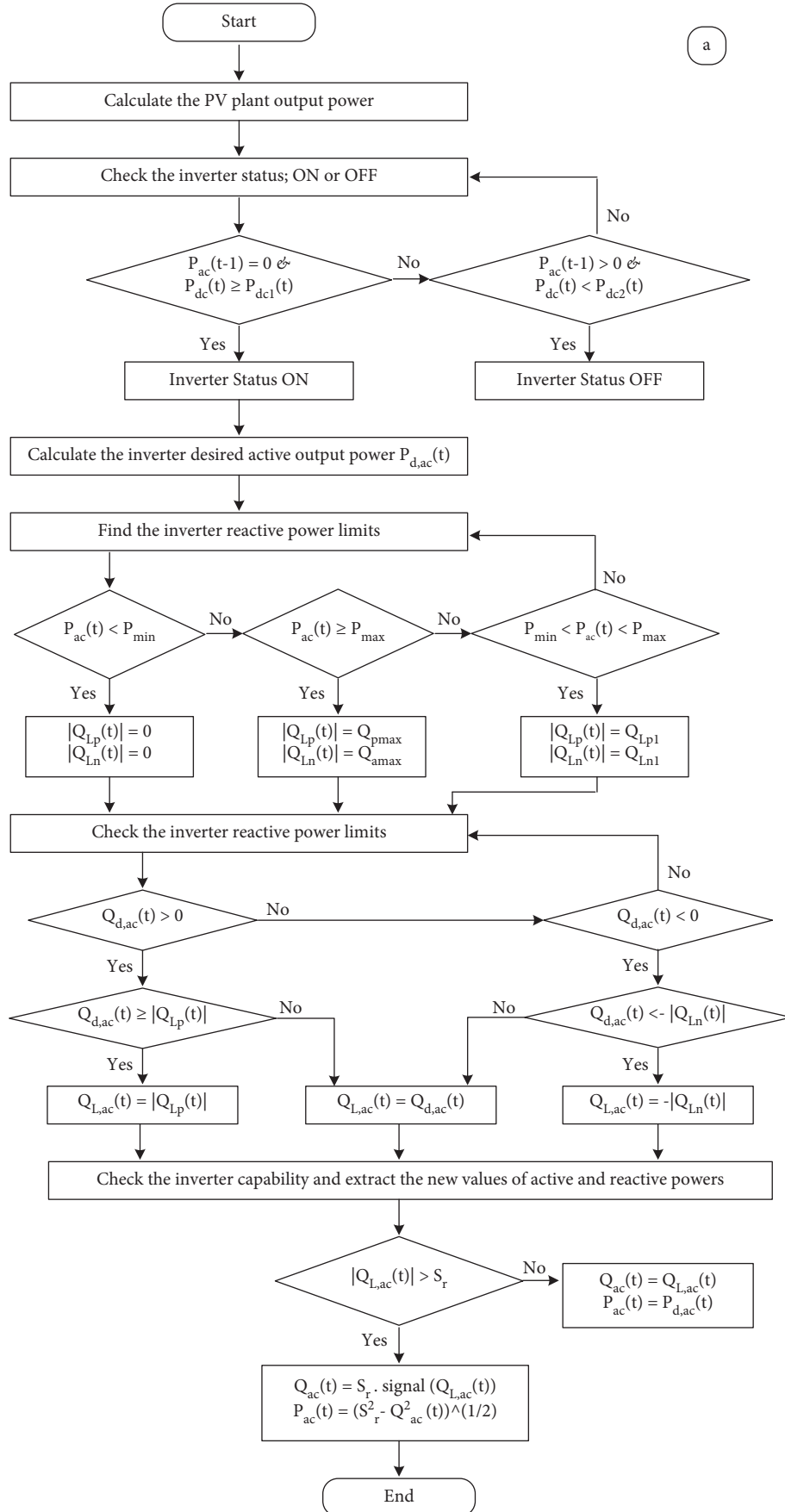


FIGURE 10: Flow chart of the smart inverter control for the coordinate control strategy of the microgrid.

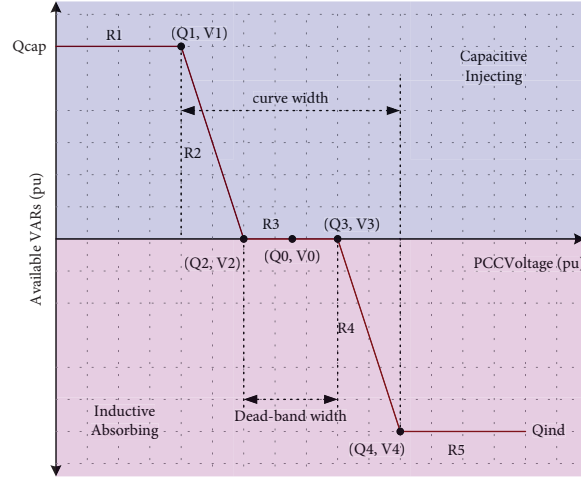


FIGURE 11: Volt-var curve for the microgrid.

$$\begin{aligned}
 Q_{d,ac}(t) \text{ if positive, } Q_{L,ac}(t) &= Q_{d,ac}(t), & \text{if } Q_{d,ac}(t) < |Q_{Lp}(t)| & |Q_{Lp}(t)|, & \text{if } Q_{d,ac}(t) \geq |Q_{Lp}(t)| \\
 &= -|Q_{Ln}(t)|, & \text{if } Q_{d,ac}(t) < -|Q_{Ln}(t)| & Q_{d,ac}(t), & \text{if } Q_{d,ac}(t) \geq -|Q_{Ln}(t)|.
 \end{aligned}
 \tag{14}$$

The reactive power limits  $Q_{Lp}(t)$  and  $Q_{Ln}(t)$  are defined by Eqs. (15) and (16) as a function of the active power delivered to the grid  $P_{ac}(t)$ :

$$|Q_{Lp}(t)| = 0, \quad \text{if } P_{ac}(t) < P_{\min} \frac{Q_{p \max}}{\% P_{\min}}. P_{ac}(t) = Q_{Lp1}, \quad \text{if } P_{\min} < P_{ac}(t) < P_{\max} Q_{p \max}, \quad \text{if } P_{ac}(t) \geq P_{\max},
 \tag{15}$$

$$|Q_{Ln}(t)| = 0, \quad \text{if } P_{ac}(t) < P_{\min} \frac{Q_{a \max}}{\% P_{\min}}. P_{ac}(t) = Q_{Ln1}, \quad \text{if } P_{\min} < P_{ac}(t) < P_{\max} Q_{a \max}, \quad \text{if } P_{ac}(t) \geq P_{\max}.
 \tag{16}$$

- (e) Check the inverter capability or the maximum inverter capacity corresponding to its KVA rating and extract the new values of active and reactive power. When the inverter capacity is not exceeded, the expressions for the active and reactive powers,  $P_{ac}(t)$  and  $Q_{ac}(t)$ , are given by the following equations:

$$P_{ac}(t) = P_{d,ac}(t), \tag{17}$$

$$Q_{ac}(t) = Q_{L,ac}(t). \tag{18}$$

However,  $P_{ac}(t)$  and  $Q_{ac}(t)$  must be reduced to meet the reactive power priority when the inverter capacity is exceeded. The reduced active power under the condition of reactive power priority is given by the following equation:

$$P_{ac}(t) = \sqrt{S_r^2 - Q_{ac}^2(t)}. \tag{19}$$

If the desired reactive power is greater than or equal to the inverter capacity ( $S_r$ ), then the new value of the reactive power becomes the capacity of the inverter itself, as given by the following equation:

Step 2: Sample the control elements: voltages at all nodes are sampled by the inverter control to verify the need for control action. When necessary, the control action is included in the inverter control list.

Step 3: Execute the inverter control action for  $t$  and update the reactive power of the PV plant. The desired reactive power is calculated according to the predefined smart inverter volt-var function, calculated for the present monitored voltage using a predefined curve (Figure 11).

## 6. Results and Discussion

This paper investigated the performance analysis of the proposed SI-CB control strategy during several PV penetrations in 11 buildings in the MG test model for two days from January 1 to 2, 2015. The MG test model was designed

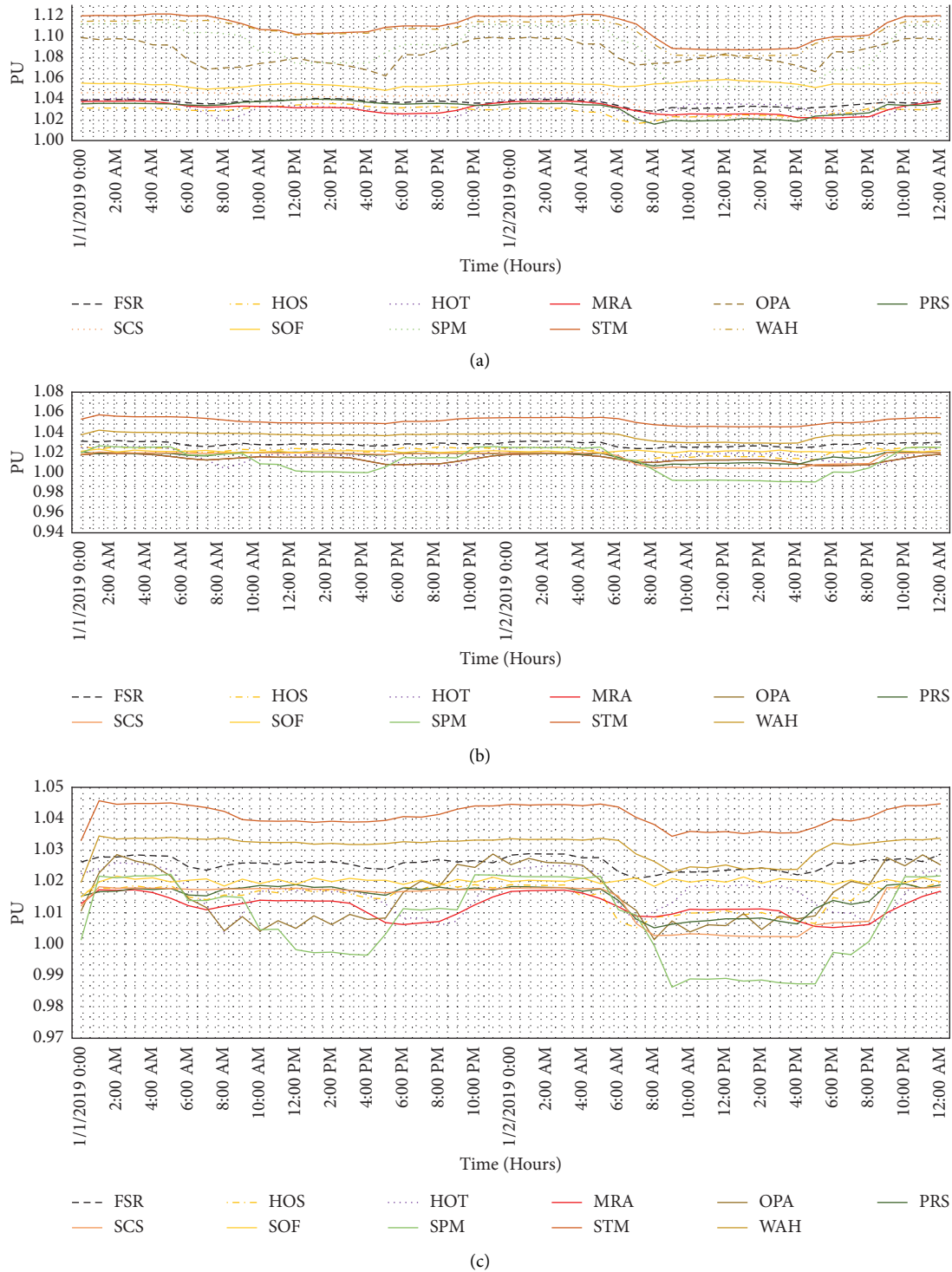


FIGURE 12: (a) Per unit voltages of 11 loads under 100% PV without control. (b) Per unit voltages of all loads with 100% PV with smart inverter control. (c) Voltages of all loads with 100% PV with smart inverter and capacitor bank control.

using the OpenDSS software platform with MATLAB. Our proposed SI-CB control strategy was verified via the following five cases.

6.1. Case 1. Compare three approaches per unit (V) for 100% PV penetration in 11 buildings in the MG test model (Figure 12).

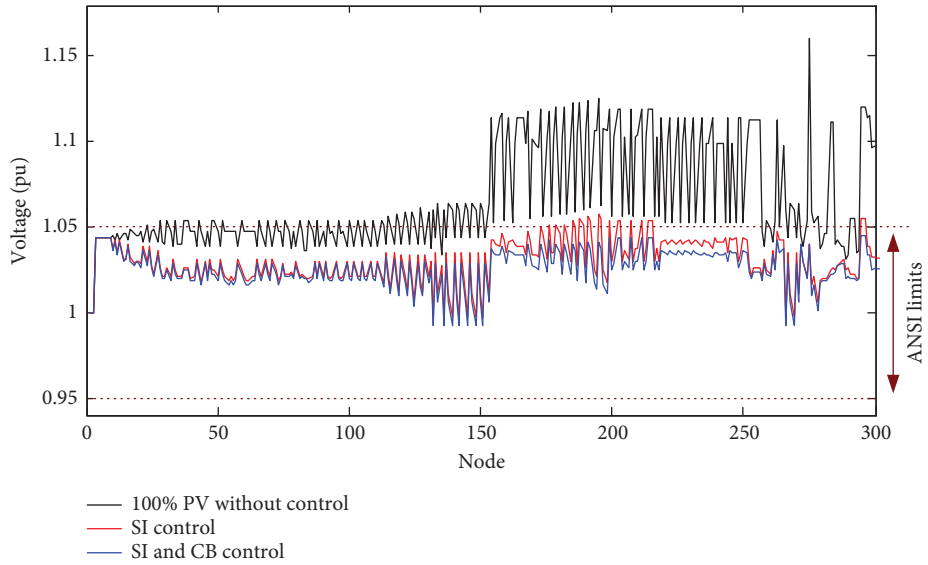


FIGURE 13: Per unit voltage vs. feeder nodes in the test grid.

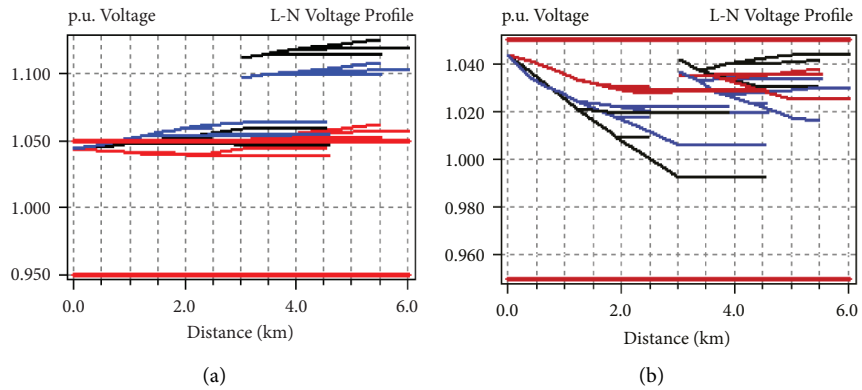


FIGURE 14: Per unit voltage vs. distance: (a) 100% PV without control and (b) 100% PV with the SI and CB control.

TABLE 5: FVSI for PV power generation levels in the microgrid: (a) 45%, (b) 60%, (c) 100%, and (d) 200% on January 2, 2019, at 2:00 p.m., considering the load defined in Figure 1.

Building	FVSI with SI-CB control			
	(a) 45% PV power generation	(b) 60% PV power generation	(c) 100% PV power generation	(d) 200% PV power generation
FSR	0.0586	0.059	0.059	0.0591
HOS	0.2129	0.219	0.2165	0.2163
HOT	0.6403	0.6401	0.6536	0.6738
MRA	0.0532	0.0529	0.0533	0.053
OPA	0.1787	0.1789	0.1673	0.1649
PRS	0.1908	0.1921	0.1916	0.1917
SCS	0.2181	0.2171	0.2185	0.2165
SOF	0.2125	0.2186	0.2161	0.2159
SPM	0.2541	0.2491	0.2594	0.2533
STM	0.0695	0.0695	0.0691	0.0692
WAH	0.1035	0.103	0.1035	0.1019

TABLE 6: Total power loss from January 1 to 2, 2015, for three approaches.

Scenario (1/2/2015, 2:00 p.m.)	Total P loss (kW)
100% PV	7
100% PV with SI	37
100% PV with SI and CB	35

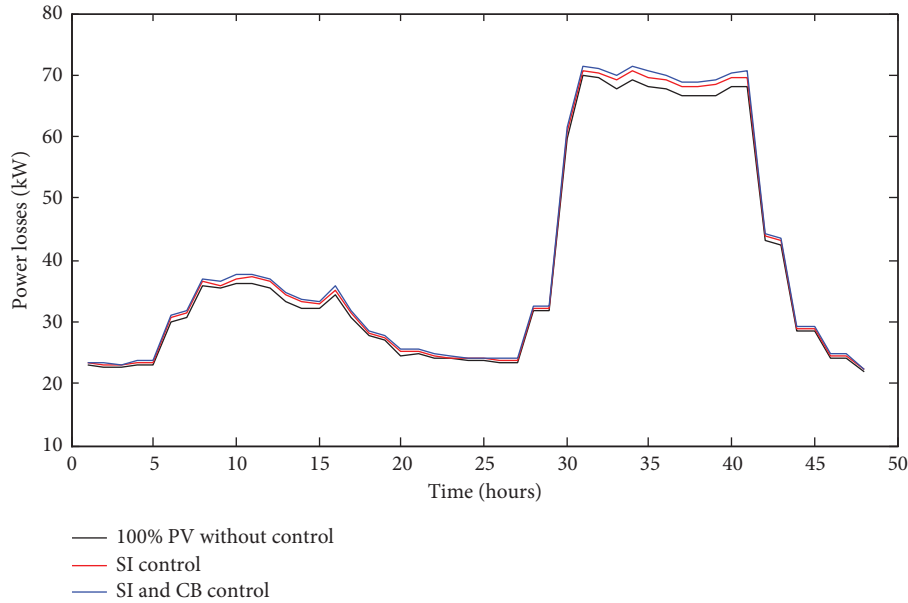


FIGURE 15: Power loss versus nodes for HOS load.

6.2. *Case 2.* Compare three approaches per unit (V) for each node in the MG test model during 100% of PV penetration (Figure 13).

6.3. *Case 3.* Determine the voltage stability to maintain the range of the ANSI limits versus distance per unit (V) and line for the voltage profile for reference and PV with SI-CB control during 100% PV power generation (Figure 14).

6.4. *Case 4.* Determine the best place for PV installation with SI-CB control in terms of the FVSI for four different levels of PV power generation (Table 5).

6.5. *Case 5.* Evaluate the total power loss (kW) for comparison between 100% PV with SI control and SI-CB control for two days (Table 6).

Figure 12 illustrates a voltage per unit of all loads in the MG under 100% PV with three different approaches: (a) without control, (b) with SI control, and (c) with SI-CB control. In conjunction with Figure 12(a), Figure 12(b) illustrates that the voltage profiles per unit also maintain acceptable voltages at all points along the distribution feeder between 0.95 and 1.05, except the STM load by applying the proposed controls. Moreover, Figure 12(c) illustrates the improved voltage profiles compared to when the coordinated control of the proposed SI-CB has not been enacted for the STM load.

Most utilities in the US follow the ANSI voltage standards [46] to maintain acceptable service voltages. The service voltage is the point where the electrical systems of the supplier and user are interconnected, which is normally at a smart meter. According to the ANSI standard, the service voltages should be within  $\pm 5\%$  of the nominal voltage level

(240 V), which translates to 0.95 to 1.05 per unit voltage [47]. Figure 13 indicates that SI control and SI-CB control can improve voltage stability to maintain the ANSI limits for each node during 100% PV power generation in the MG. However, SI control exceeds the 1.05 per unit in the node from 170 to 110 and after 280 nodes during this period. The baseline voltage profile along the feeder with 100% PV with no control reveals that the voltage profile exceeds ANSI (1.05), as depicted in Figure 14. After applying the SI-CB control of PV, the voltage profile is maintained in the range of ANSI limits (0.95–1.05 per unit).

The line with an FVSI close to 1.00 indicates that it is approaching instability; hence, one of the buses to connect this line will experience a sudden voltage drop, leading to voltage collapse. The FVSI of all the lines must be lower than 1 to ensure the stability of the power system. Table 5 indicates the best FVSI for each installation place for each PV power generation. In Table 5, MRA is the best place to install PV with SI-CB control for all cases, whereas HOT is the worst case on January 2, 2019, at 2:00 p.m.

When the grid is connected to PV, used in SI control, it results in a power-loss increase. Figure 15 and Table 6 demonstrate that the total power loss in PV with SI control increased slightly by 30 kW compared to without control (100% PV only) at 7 kW. Furthermore, the proposed strategy (100% PV with SI-CB) has slightly (2 kW) less than only SI control (100% PV with SI).

## 7. Conclusion

In this paper, a coordinate strategy based on SIs and CB control was proposed to mitigate the high PV energy penetration in a modified IEEE 123-node test feeder. The main contribution is to provide a comprehensive approach



enhancing the proposed MG configuration in terms of voltage stability and ANSI standards. The proposed approach was achieved using the parallel processing of MATLAB and OpenDSS. Thus, several actual commercial buildings were connected to different buses, and actual weather data were considered to conduct a real feeder operation. Different cases of MG operation were considered for testing the robustness of the proposed algorithm for voltage mitigation. When the grid is connected to PV, the proposed strategy (100% PV with SI-CB) has slightly (2 kW) less than only SI control (100% PV with SI). MRA is the best place to install PV as 0.05 with SI-CB control for all cases, whereas HOT is the worst case as 0.64 on January 2, 2019, at 2:00 p.m. in terms of FVSI. The results prove its effectiveness when dealing with a high penetration level of PV power generation, controlling the SI and CB. The voltage stability was assessed using several metrics, such as power loss and the FVSI, which was less than 1 for the four studied cases. Thus, in all feeder nodes, the pu voltage was maintained in the range of ANSI limits (0.95–1.05 per unit) despite the different sever operation conditions because of the high level of PV penetration. In addition, particular interest was given to the simulation part by presenting essential steps to perform such a study. The presented work can be extended to perform studies for other feeders. The presented work can be extended to study other solutions such as integration of high-power storage solutions or fuel cells. Adding to the power criteria, other physical aspects related to the management of their dynamics, temperatures, and their best economic use are to be investigated. In addition, it is interesting to provide a comprehensive comparison study with other voltage mitigation techniques for the use of the OpenDSS tool to develop benchmarks for microgrid tests.

## Abbreviations

$T_c$ :	Cell temperature inside the module ( $^{\circ}\text{C}$ )
$T_m$ :	Measured back-surface module temperature ( $^{\circ}\text{C}$ )
$I_r$ :	Measured solar irradiance on module ( $\text{W}/\text{m}^2$ )
$T_a$ :	Ambient air temperature ( $^{\circ}\text{C}$ )
$I_{r0}$ :	Reference solar irradiance on module ( $1000 \text{ W}/\text{m}^2$ )
$WS$ :	Wind speed measured at a standard 10 m height (m/s)
$\Delta T$ :	Temperature difference between the cell and module back surface at an irradiance level of $1000 \text{ W}/\text{m}^2$
$a$ :	Empirically determined coefficient establishing the upper limit for the module temperature at low wind speeds and high solar irradiance
$b$ :	Empirically determined coefficient establishing the rate at which the module temperature drops as the wind speed increases
$P_{mpp}$ :	Max power point power at a selected temperature of $25^{\circ}\text{C}$ and an irradiance of $1.0 \text{ kW}/\text{m}^2$
$f$ :	Correction factor versus temperature variation: $f$ is defined as when the panel temperature

increases from  $25^{\circ}\text{C}$  to  $75^{\circ}\text{C}$ , the power drops by about 22%

$P_{PV,n}$ :	Real power when only the PV power plant is used
$Q_{PV,n}$ :	Reactive power when only the PV power plant is used
$P_{PS,n}$ :	Real power when a smart inverter of solar PV is installed
$Q_{PS,n}$ :	Reactive power when a smart inverter of solar PV is installed
$P_{CB,n}$ :	Real power from the smart inverter of solar PV with CB
$Q_{CB,n}$ :	Reactive power from the smart inverter of solar PV with CB
$P_n$ :	Complex real power flow
$Q_n$ :	Complex reactive power flow
$V_n$ :	The magnitude of the voltage at node $n$
$S_r$ :	Inverter's kVA rating
$\%S_{r1}$ :	Percentage of inverter's kVA rating. When the inverter is off, the power from the PV array (DC power) must be greater than this value for the inverter to turn on
$\%S_{r2}$ :	Percentage of inverter's kVA rating. When the inverter is on, it turns off when the power from the array (DC power) drops below this value
$E_{curve}$ :	Inverter efficiency curve, characterizing the variation of the inverter efficiency as a function of the power from the PV array, $P_{dc}$ , per unit of inverter's kVA rating
$Q_{Lp}$ :	Reactive power positive limit when provided
$Q_{Ln}$ :	Reactive power negative limit when absorbed
$Q_{pmax}$ :	Maximum value of reactive power that the inverter can provide to the grid
$Q_{amax}$ :	Maximum value of reactive power that the inverter can absorb from the grid
$\%$	Percentage of the $P_{mpp}$ . The inverter cannot provide/absorb reactive power when its active output power is less than this value
$P_{min}$ :	Percentage of the $P_{mpp}$ . The inverter cannot provide/absorb reactive power up to its maximum allowed value, $Q_{pmax}$ or $Q_{amax}$ , respectively, when its active output power is greater than this value.

## Data Availability

Data are available upon request.

## Conflicts of Interest

The authors declare that they have no conflicts of interest.

## Acknowledgments

This research project was supported in part by PAQ-Colabora (PAR&I-Tk), 2019–2022 program managed by the Tunisian Ministry of High Education and Scientific Research under Grant LSE-ENIT-LR11ES15. This research was also

supported by the Basic Study and Interdisciplinary R&D Foundation Fund of University of Seoul (2021).

## References

- [1] S. Lenhart and K. Araújo, "Microgrid decision-making by public power utilities in the United States: a critical assessment of adoption and technological profiles," *Renewable and Sustainable Energy Reviews*, vol. 139, no. C, 2021.
- [2] E. Prehoda, C. Schelly, and J. U. S. Pearce, "Strategic solar photovoltaic-powered microgrid deployment for enhanced national security," *Renewable and Sustainable Energy Reviews*, vol. 78, pp. 167–175, 2017.
- [3] M. Warneryd, M. Hakansson, and K. Karltorp, "Unpacking the complexity of community microgrids: a review of institutions' roles for development of microgrids," *Renewable and Sustainable Energy Reviews*, vol. 121, Article ID 109690, 2020.
- [4] X. Lu, S. Bahramirad, J. Wang, and C. Chen, "Bronzeville community microgrids: a reliable, resilient and sustainable solution for integrated energy management with distribution systems," *The Electricity Journal*, vol. 28, no. 10, pp. 29–42, 2015.
- [5] F. S. El-Faouri, M. W. Alzadhan, M. G. Batarseh, A. Mohammad, and M. E. Za'ter, "Modeling of a microgrid's power generation cost function in real-time operation for a highly fluctuating load," *Simulation Modelling Practice and Theory*, vol. 94, pp. 118–133, 2019.
- [6] N. Chettibi and A. Mellit, "FPGA-based real time simulation and control of grid-connected photovoltaic systems," *Simulation Modelling Practice and Theory*, vol. 43, pp. 34–53, 2014.
- [7] M. Bourogaoui, A. Houari, H. B. AttiaSethom, and M. Machmoum, "A novel technique for online resonance frequencies monitoring based on wavelet transform for grid-connected solar inverters," *Electric Power Systems Research*, vol. 199, 2021.
- [8] M. Kharrich, O. H. Mohammed, N. Alshammari, and M. Akherraz, "Multi-objective optimization and the effect of the economic factors on the design of the microgrid hybrid system," *Sustainable Cities and Society*, vol. 65, Article ID 102646, 2021.
- [9] M. Daneshvar, B. Mohammadi-Ivatloo, K. Zare, and S. Asadi, "Transactive energy management for optimal scheduling of interconnected microgrids with hydrogen energy storage," *International Journal of Hydrogen Energy*, vol. 46, no. 30, pp. 16267–16278, 2021.
- [10] C. Liu, Y. Qin, and H. Zhang, "Real-time scheduling strategy for microgrids considering operation interval division of DGs and batteries," *Global Energy Interconnection*, vol. 3, no. 5, pp. 442–452, 2020.
- [11] *IEEE Recommended Practice for Utility Interface of Photovoltaic (PV) Systems*, IEEE, Piscataway, NJ, USA, 2000.
- [12] *IEEE Standard for Interconnecting Distributed Resources with Electric Power Systems*, IEEE, Piscataway, NJ, USA, 2003.
- [13] *Microgrid-Ready Solar PV-Planning for Resiliency*, <https://www.nrel.gov/docs/fy18osti/70122.pdf>, 2017.
- [14] S. Newman, K. Shiozawa, J. Follum et al., "A comparison of PV resource modeling for sizing microgrid components," *Renewable Energy*, vol. 162, pp. 831–843, 2020.
- [15] K. Nwaigwe, P. Mutabilwa, and E. Dintwa, "An overview of solar power (PV systems) integration into electricity grids," *Materials Science for Energy Technologies*, vol. 2, no. 3, pp. 629–633, 2019.
- [16] J. Kaushal and P. Basak, "Power quality control based on voltage sag/swell, unbalancing, frequency, THD and power factor using artificial neural network in PV integrated AC microgrid," *Sustainable Energy, Grids and Networks*, vol. 23, Article ID 100365, 2020.
- [17] A. Kulmala, S. Repo, and P. Järventausta, "Coordinated voltage control in distribution networks including several distributed energy resources," *IEEE Transactions on Smart Grid*, vol. 5, no. 4, pp. 2010–2020, 2014.
- [18] R. Broderick, J. Quiroz, M. Reno, A. Ellis, J. Smith, and R. Dugan, "Time series power flow analysis for distribution connected PV generation," *Technical Report*, 2013.
- [19] K. P. Schneider, B. A. Mather, B. C. Pal et al., "Analytic considerations and design basis for the IEEE distribution test feeders," *IEEE Transactions on Power Systems*, vol. 99, 2017, <https://site.ieee.org/pes-testfeeders/resources/>.
- [20] T. A. Marulanda and A. Pavas, "Simulation of modern distribution systems using MATLAB and OpenDSS," in *Proceedings of the fise-IEEE/CIGRE Conference Living the Energy Transition*, 2019.
- [21] J. A. Ahamioje and H. Krishnaswami, "Interconnection study of distributed PV systems by interfacing MATLAB with OpenDSS and GIS," in *Proceedings of the IEEE 44th Photovoltaic Specialist Conference*, 2017.
- [22] S. K. Solanki, V. Ramachandran, and J. Solanki, "Steady state analysis of high penetration PV on utility distribution feeder," in *Proceedings of the PES T&D 2012*, 2012.
- [23] J. Ma, F. Yang, Z. Li, and S. J. Qin, "A renewable energy integration application in a microgrid based on model predictive control," in *Proceedings of the IEEE Power and Energy Society General Meeting*, 2012.
- [24] S. Pukhrem, *Investigation into Photovoltaic Distributed Generation Penetration in the Low Voltage Distribution Network*, Technological University Dublin, Dublin, Ireland, 2019.
- [25] V. Ramachandran, *Modeling of Utility Distribution Feeder in OpenDSS with Steady State Impact Analysis of Distributed Generation*, West Virginia University, Morgantown, West VA, USA, 2011.
- [26] S. Nowak, M. S. Metcalfe, W. Eberle, and L. Wang, "Comparison of voltage control methods in distribution systems using Q-V based PI and droop controls of solar inverters," in *Proceedings of the IEEE Power & Energy Society General Meeting*, 2017.
- [27] H. J. Liu and T. J. Overbye, "Smart-grid-enabled distributed reactive power support with conservation voltage reduction," in *Proceedings of the Power and Energy Conference at Illinois*, 2014.
- [28] Y. Liu, Y. Tai, C. Huang, H. Su, P. Lan, and M. Hsieh, "Assessment of the PV hosting capacity for the medium-voltage 11.4kV distribution feeder," in *Proceedings of the IEEE International Conference on Applied System Invention*, 2018.
- [29] M. Ammar and A. M. Sharaf, "Optimized use of PV distributed generation in voltage regulation: a probabilistic formulation," *IEEE Transactions on Industrial Informatics*, vol. 15, no. 1, pp. 247–256, 2019.
- [30] <https://www.energy.gov/eere/buildings/commercial-reference-buildings>, 2022.
- [31] O. P. Mahela, B. Khan, H. H. Alhelou, S. Tanwar, and S. Padmanaban, "Harmonic mitigation and power quality improvement in utility grid with solar energy penetration using distribution static compensator," *IET Power Electronics*, vol. 14, no. 5, pp. 912–922, 2021.
- [32] A. Chaves and A. Terry Bahill, "Comparison of risk analysis approaches and a case study of the risk of incorporating solar

- photovoltaic systems into a commercial electric power grid,” *Systems Engineering*, vol. 17, no. 1, pp. 89–111, 2014.
- [33] S. Charadi, Y. Chaibi, A. Redouane, A. Allouhi, A. el Hasnaoui, and H. Mahmoudi, “Efficiency and energy-loss analysis for hybrid AC/DC distribution systems and microgrids: a review,” *International Transactions on Electrical Energy Systems*, vol. 31, no. 12, Article ID e13203, 2021.
- [34] E. A. Hamza, B. E. Sedhom, and E. A. Badran, “Impact and assessment of the overvoltage mitigation methods in low-voltage distribution networks with excessive penetration of PV systems: a review,” *International Transactions on Electrical Energy Systems*, vol. 31, no. 12, Article ID e13161, 2021.
- [35] <https://ec.europa.eu/jrc/en/pvgis>, 2022.
- [36] J. Kratochvil, W. E. Boyson, and D. King, “Photovoltaic array performance model,” *Sandia Reports*, pp. 8–19, 2004.
- [37] <https://power.larc.nasa.gov/data-access-viewer/>, 2022.
- [38] *Electric Power Research Institute, OpenDSS Cheatsheet: Examples of Commonly-Used OpenDSS Commands*, <https://www.epri.com/pages/sa/opendss>, 2014.
- [39] C. G. Sain, *An OpenDSS Implementation of a Generic Municipal Microgrid for Co-simulation*, <https://core.ac.uk/download/pdf/227472351.pdf>, 2019.
- [40] M. E. Baran and F. F. Wu, “Network reconfiguration in distribution systems for loss reduction and load balancing,” *Transactions on Power Delivery*, vol. 4, no. 2, pp. 1401–1407, 1989.
- [41] H. Li, C. Wen, K.-H. Chao, and L.-L. Li, “Research on inverter integrated reactive power control strategy in the grid-connected PV systems,” *Energies*, vol. 10, no. 7, p. 912, 2017.
- [42] M. Jaszczur and Q. Hassan, “An optimisation and sizing of photovoltaic system with supercapacitor for improving self-consumption,” *Applied Energy*, vol. 279, no. C, Article ID 115776, 2020.
- [43] T. Funabashi, J. Liu, and T. Senjyu, “Stability problems of distributed generators,” *Integration of Distributed Energy Resources in Power Systems*, pp. 261–281, 2016.
- [44] A. Arabali, M. Ghofrani, J. B. Bassett, M. Pham, and M. Moeini-Aghataei, “Optimum sizing and siting of renewable-energy-based DG units in distribution systems,” *Optimization in Renewable Energy Systems*, pp. 233–277, 2017.
- [45] N. Hosseinzadeh, A. Aziz, A. Mahmud, A. Gargoom, and M. Rabbani, “Voltage stability of power systems with renewable-energy inverter-based generators: a review,” *Electronics*, vol. 10, no. 2, p. 115, 2021.
- [46] *Enhancing Distribution Resiliency—Opportunities for Applying Innovative Technologies*, Electric Power Research Institute, Washington, DC, USA, 2013.
- [47] H. V. Padullaparti, P. Chirapongsananurak, S. Santoso, and J. A. Taylor, “Edge-of-grid voltage control: device modeling, strategic placement, and application considerations,” *IEEE Power and Energy Technology Systems Journal*, vol. 4, pp. 106–114, 2017.